Diffuse reflectance imaging for non-melanoma skin cancer detection using laser feedback interferometry

Alireza Mowla[a], Thomas Taimre[b], Yah Leng Lim[a], Karl Bertling[a], Stephen J. Wilson[a], Tarl W. Prow[c], H. Peter Soyer[c], and Aleksandar D. Rakić[a]

[a]The University of Queensland, School of Information Technology and Electrical Engineering, St. Lucia, Brisbane, Australia, 4072
[b]The University of Queensland, School of Mathematics and Physics, St. Lucia, Brisbane, Australia, 4072
[c]The University of Queensland, Dermatology Research Centre, School of Medicine, Translational Research Institute, Brisbane, Australia, 4102

ABSTRACT

We propose a compact, self-aligned, low-cost, and versatile infrared diffuse-reflectance laser imaging system using a laser feedback interferometry technique with possible applications in *in vivo* biological tissue imaging and skin cancer detection. We examine the proposed technique experimentally using a three-layer agar skin phantom. A cylindrical region with a scattering rate lower than that of the surrounding normal tissue was used as a model for a non-melanoma skin tumour. The same structure was implemented in a Monte Carlo computational model. The experimental results agree well with the Monte Carlo simulations validating the theoretical basis of the technique. Results prove the applicability of the proposed technique for biological tissue imaging, with the capability of depth sectioning and a penetration depth of well over 1.2 mm into the skin phantom.

Keywords: Steady state diffuse reflectance imaging, laser feedback interferometry, non-melanoma skin cancer detection, agar gel skin tissue phantom

1. INTRODUCTION

The low electromagnetic absorption of water and hemoglobin in the near-infrared spectrum has made this spectral region optimal for non-invasive *in vivo* optical interrogation of biological tissues for diagnostic purposes.[1] In the past few decades an extended range of non-invasive optical techniques, using this spectral window, have been suggested and developed to be used for non-melanoma skin cancer (NMSC), also known as keratinocyte skin cancer (KSC)*, detection. Diffuse reflectance spectroscopy has been used to determine the *in vivo* optical properties (scattering and absorption coefficients) of KSCs for diagnostics, showing that KSCs altered the optical properties of skin tissue.[2] On the other hand, *in vitro* measurement of these properties is more easily carried out and has been measured using spectrophotometers in combination with integrating spheres to look at the diffuse reflectance and total transmittance of light in biopsy samples.[3] Reduction in scattering and absorption coefficients have also been reported in KSCs, by *in vitro* measurement of diffuse reflectance and total transmittance of cancerous samples.[4]

Most biological tissues are highly scattering over the near-infrared spectral window and light will diffuse quickly as soon as it enters the tissue.[5] Therefore, optical properties of a biological tissue can be investigated by monitoring the diffuse reflectance of light from the tissue and can also be analyzed to distinguish between tumorigenic and nontumorigenic cells.[6] Detecting diffuse reflectance to measure *in vivo* optical properties of a biological sample has usually been achieved by illuminating a larger area on the tissue using an optical source and looking at the reflectance by means of a charge-coupled device camera,[7] or by transmitting light into the tissue using an optical fiber and collecting the reflected light using an arrangement of other optical fibers located near the source fiber,[8] or by focusing a beam on the biological tissue and collecting the reflected light in a confocal

*KSC and NMSC can be used interchangeably and both encompass basal cell carcinoma and squamous cell carcinoma.

Biophotonics: Photonic Solutions for Better Health Care V, edited by Jürgen Popp, Valery V. Tuchin, Dennis L. Matthews, Francesco Saverio Pavone, Proc. of SPIE Vol. 9887, 98870T
 · doi: 10.1117/12.2227449

detection scheme.[9–11] We propose a new technique based on the latter scheme which can be used in *in vivo* measurement of diffuse reflectance in the near-infrared range.

The technique proposed here is a laser feedback interferometry (LFI) system (based on self-mixing effect[12–14]) in a confocal laser feedback configuration.[15,16] In this system a near-infrared laser diode acts as both transmitter and receiver of the optical signal. The illuminating laser beam is focused on a target. A portion of the diffuse reflected light makes its way back into the laser cavity and affects the intra-cavity optical field. When the laser beam is modulated appropriately, these changes in the intra-cavity optical field due to diffuse reflected light can be measured. The focused beam is then raster scanned over the target yielding a spatially resolved image of the diffuse reflectance.

To examine the technique we applied it to two models: (1) a physical skin phantom and (2) a numerical model using Monte Carlo (MC) simulation. The physical model was a simple three-layer agar gel skin phantom containing a cylindrical 4 mm diameter region (representing a KSC). The tumorous region was included in the second layer which resembled dermis and the diameter size was in the range of a typical skin tumorous lesion.[17,18] This model was based on an approximate geometry for a typical skin with typical optical properties[19] and lower scattering coefficient in the tumorous area as it was reported by Salomatina *et al.*[4] The numerical model was a MC photon transport model, mimicking the physical skin phantom and the geometry of the experimental set up.

The paper is structured as follows: we discuss the fundamentals of LFI in Sec. 2. Skin phantom preparation procedure is presented in Sec. 3 and details about the experiment are outlined in Sec. 4. Experimental results are presented in Sec. 5 which is followed by MC simulation results in Sec. 6. Finally, we conclude in Sec. 7.

2. LASER FEEDBACK INTERFEROMETRY

Laser feedback interferometry works is on the self-mixing effect.[12–14] Self-mixing effect occurs when light emitted from the laser is reflected off a distant target and is reinjected into the laser cavity which perturbs the operation of the laser. This perturbation can contain information of interest relating to the target.

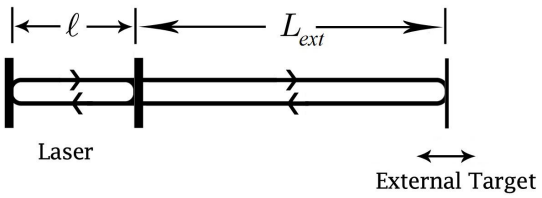

Figure 1. Three mirror model of laser in the presence of external target.

One way to study the self-mixing effect is to assume a three-mirror model instead of a conventional two-mirror model to examine the laser resonator cavity operation in the presence of an external target which can be defined as the third mirror. A schematic diagram of this model can be seen in Fig. 1. In this figure, l is the laser cavity length and L_{ext} is the distance between the exit mirror of the laser and the target. Lasing conditions in a free running laser (two-mirror model) are for the beam to have the same phase and unit gain coefficient after one round trip between the mirrors. When there is an external target in the vicinity of the laser so that a portion of the beam reflects back into the cavity, parameters of the laser are perturbed. In particular, the frequency of the free running laser shifts in order to maintain a modified phase condition for the new situation. The shift in the frequency has to satisfy the following modified phase equation (at timescales far slower than that of the internal laser dynamics):[20]

$$0 = 2\pi\tau_{\text{ext}}(\nu - \nu_0) + C\sin(2\pi\nu\tau_{\text{ext}} + \arctan\alpha)\,, \tag{1}$$

where τ_{ext} is the external round-trip time, ν is the frequency of the laser with optical feedback, ν_0 is the frequency of the free running laser in the absence of the external target, C is the feedback parameter which depends on

the level of optical feedback,[21] and α is the linewidth enhancement factor.[22] The equation for the feedback parameter C is as follows:[20]

$$C = \frac{\tau_{\text{ext}}}{\tau_\ell}\,\kappa_{\text{ext}}\,\sqrt{1+\alpha^2}\,, \tag{2}$$

where τ_ℓ is the intra-cavity round-trip time, and κ_{ext} is the coupling coefficient which is a function of reflectivity of the target and exit laser mirror as follows:[20]

$$\kappa_{\text{ext}} = \varepsilon\sqrt{\frac{R_{\text{ext}}}{R_s}}\,(1-R_s)\,, \tag{3}$$

where ε is the fraction of the reflected beam which coherently coupled back into the lasing mode,[21] and R_{ext} and R_s are the reflectivities of the target and exit laser mirror, respectively. By defining the external round-trip phase in the presence of the target as $\varphi = 2\pi\nu\tau_{\text{ext}}$ and external round-trip phase in the absence of the target as $\varphi_0 = 2\pi\nu_0\tau_{\text{ext}}$, Eq. (1) can be written in the following form:[20]

$$0 = \varphi - \varphi_0 + C\sin(\varphi + \arctan\alpha)\,. \tag{4}$$

Solving Eq. (4) for φ is not trivial as there is no closed-form solution for it. After solving this equation numerically, perturbation in the threshold gain of the laser due to the optical feedback can be formulated as:[20]

$$\Delta g_{\text{th}} = -\frac{\kappa_{\text{ext}}}{L}\cos(\varphi)\,, \tag{5}$$

where L is the target distance from the laser. The variations in g_{th} can then cause an observable fluctuation in the laser optical power which is caused by the changes in the external round-trip phase in the presence of a target, as:

$$\Delta P = \beta\cos(\varphi)\,, \tag{6}$$

where β is the amplitude of self-mixing signal which is dependent on the laser and system parameters (such as the amount of light being coupled back into the laser cavity, the distance to the target, and the photon lifetime in the laser cavity). The characteristics of the external target can then be sensed by monitoring the changes in the optical output power of the laser or changes in the terminal voltage of the laser.[16] In this paper we used a vertical cavity surface emitting laser (VCSEL) and measured the laser terminal voltage, from which we derive our self-mixing signal.[23] Therefore, the proposed LFI system is compact and low-cost as VCSELs can be provided in small dimensions and inexpensively.

3. SKIN PHANTOM

Optical properties of human skin have been studied extensively for the purposes of diagnosis, treatment, and improved understanding of health and disease mechanisms.[3,19] Human skin consists of three main layers: epidermis, dermis, and subcutaneous tissue. Epidermis contains mostly keratinocytes and no blood vessels though it does contain melanocytes as well. Melanocytes are the melanin producing cells. Melanin is a pigment which is the main absorber of light and is located above the nuclei of keratinocytes along the epidermal basal cell layer protecting the nuclear DNA from harmful ultra-violet irradiation. Dermis contains blood vessels, lymphatics, nerves, and two types of fibers: collagen and elastic fibers. Dermis is an optically turbid medium with a scattering coefficient much higher than its absorption coefficient as it normally does not contain any melanin[24] and it is also much thicker than epidermis. Subcutaneous tissue is the lowermost layer of the human skin which mainly consists of fat cells.

Agar is a matrix hydrogel material consists of a network of hydrophilic polymers. It is mainly made up of water and is a biologically and biochemically compatible material which has already been used as tissue phantoms.[25,26] Agar gel has innate optical properties which depend on the purity and concentration of the agar powder in the gel. Scattering and absorption coefficients of a pure agar gel are usually low and to control the scattering and absorption coefficients of the agar gel in a phantom, material to specifically modify the scattering and absorption must be added to the agar gel. We added titanium dioxide (TiO_2) and instant coffee to the agar gel to control its optical properties. Titanium dioxide powder is widely accepted as a scatterer in the

near-infrared range[26] which is inexpensive and safe. Instant coffee can also be used as a good absorber of light in this frequency range.[27]

The agar skin tissue phantom in this paper contained three layers. Figure 2 illustrates steps in making the agar gel skin phantom. All the layers were placed on a 150 μm thick cover slip individually. This cover slip on the top of the agar tissue phantom stopped agar from evaporation and held the sample relatively static. In Fig. 2(a) the outermost layer which was a 500 μm thick 1.2% weight to weight (w/w) agar gel doped with 1.2% w/w instant coffee powder was placed on the cover slip. This layer resembled epidermis (although epidermis is usually between 80 to 120 μm thick, to avoid complexity in making such a thin agar layer, we approximated this layer to be 500 μm) which is high in melanin concentration. Fig. 2(b) shows the second layer which was a 1000 μm thick 1.2% w/w agar gel doped with about 0.1% w/w TiO_2 powder on top of the first layer. This layer had a high scattering feature and it resembled dermis which is highly scattering. We punched out a 4 mm diameter cylindrical area in the middle of this layer and replaced it with a 4 mm diameter cylindrical layer made up of pure 1.2% w/w agar gel with the same thickness of 1000 μm, to approximately resemble a KSC area. Based on our measurements in this section, the scattering coefficient of this cancerous area is about 0.3 of the scattering coefficient of the surrounding second layer. This typical drop factor in the scattering coefficient of the cancerous area is consistent with the measured drops in the scattering coefficients of three type of KSCs, which are reported to be about 0.5, 0.03, and 0.005 for infiltrative basal cell carcinoma, nodular basal cell carcinoma, and squamous cell carcinoma, respectively, at the wavelength of 850 nm, with respect to that of a healthy dermis.[4] Third layer was a thicker pure agar gel layer which resembled subcutaneous tissue with relatively lower scattering and absorption coefficients. Fig. 2(c) shows the third layer which was a 3.15 mm thick pure 1.2% w/w agar gel on top of the second layer. We wrapped the bottom side with a piece of plastic to stop agar from evaporating and make the sample more stable. Finally the top view of the sample is shown in Fig. 2(d).

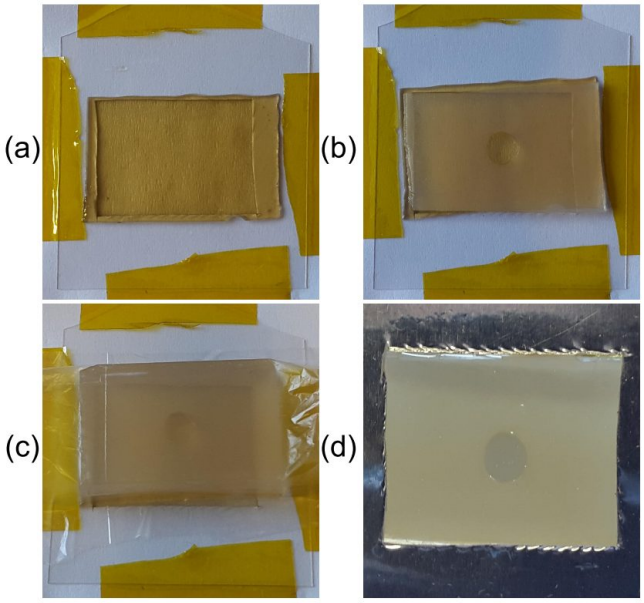

Figure 2. Agar skin tissue phantom; (a) a high absorptive 500 μm layer on a 150 μm thick cover slip resembling the epidermis, (b) a high scattering 1000 μm layer enclosing a 4 mm diameter cylindrical lower scattering tumorous model as the equivalent of dermis, (c) 3.15 mm pure agar layer resembling the subcutaneous tissue and a plastic wrap, (d) top view of the skin phantom.

The agar gel was prepared by dissolving the w/w proportion of the agar powder in distilled water. The mixture was then placed in a microwave oven and heated up to the boiling point to start the polymerization process. The mixture was removed from the microwave oven as soon as it reached the boiling point and was stirred well manually for a few minutes. Instant coffee was added to the mixture according to the desired w/w proportion. Instant coffee was very soluble in the hot mixture and was easily dissolved by stirring. Titanium

dioxide in powdered form was added to the agar gel mixture as desired according to w/w proportion. Dissolving TiO_2 uniformly in the agar gel was not trivial as it was a metal oxide powder which was heavy and precipitated quickly if not stirred well. It resided in the agar gel in suspension before the gel was set and constant stirring for about 30 minutes was needed to avoid deposition and remaining in a clumpy powder form.[26] The mixture was also kept hot during the stirring process. To make a agar gel layer with specific thickness, we poured the prepared agar mixture into a Petri dish containing two microscope slides which were separated by two spacers at the ends with specific thickness as desired. The hot agar mixture spread between the two microscope slides and when solidified a layer with the required thickness was obtained.

To estimate the optical properties of the prepared layers. The agar gel layer, doped with different levels of absorber and scatterer, was illuminated with a collimated laser beam at 850 nm. Power of the collimated laser beam was recorded before and after passing through the sample. Based on the Beer–Lambert law, the total attenuation of light traveling in a transparent material depends on its optical properties, and can be described as:

$$\mu_t = -\frac{1}{L} \ln \frac{P}{P_0}\,, \tag{7}$$

where μ_t is the total attenuation of the light, L is the agar sample thickness, P is the power of the transmitted light, and P_0 is the power of the non-attenuated light. The total attenuation can also be formulated as:

$$\mu_t = \mu_{a_{\text{sam}}} + \mu_{s_{\text{sam}}}\,, \tag{8}$$

where $\mu_{a_{\text{sam}}}$ and $\mu_{s_{\text{sam}}}$ are the absorption and scattering coefficients of the sample, respectively. Optical properties of the sample can be a combination of the optical properties of the base gel and additive absorbers and scatterers based on their concentrations. In this work instant coffee and TiO_2 were used as the main absorber and scatterer. Therefore, the absorption and scattering coefficients of the sample can be written respectively as:

$$\mu_{a_{\text{sam}}} = \mu_{a_{\text{agar}}} \times C_{\text{agar}} + \mu_{a_{\text{coffee}}} \times C_{\text{coffee}}\,, \tag{9}$$

and:

$$\mu_{s_{\text{sam}}} = \mu_{s_{\text{agar}}} \times C_{\text{agar}} + \mu_{s_{\text{TiO2}}} \times C_{\text{TiO2}}\,, \tag{10}$$

where $\mu_{a_{\text{agar}}}$ and $\mu_{a_{\text{coffee}}}$ are the absorption coefficients of the agar powder and instant coffee, respectively, C_{agar} and C_{coffee} are the concentrations (volume proportion) of the agar powder and instant coffee, respectively, $\mu_{s_{\text{agar}}}$ and $\mu_{s_{\text{TiO2}}}$ are the scattering coefficients of the agar powder and TiO_2, respectively, and C_{TiO2} is the concentration (volume proportion) of TiO_2 powder in the gel.

We used a collimated laser beam at 850 nm to measure the optical properties of the samples and estimated the absorption coefficient of the pure 1.2% w/w agar gel to be equal to that of water which is also consistent with the literature[25] and was a start point for our measurements. This means we approximated C_{agar} to be about 0.01 for a 1.2% w/w agar gel and we took $\mu_{a_{\text{agar}}}$ to be 50 m^{-1}. After applying the technique to the pure agar gel, we measured the total attenuation μ_t to be 66.35 m^{-1} and considering the formula in the previous paragraph, $66.35 = 50 \times 0.01 + \mu_{s_{\text{agar}}} \times 0.01$, $\mu_{s_{\text{agar}}}$ was calculated to be 6585 m^{-1}. After calculating $\mu_{a_{\text{agar}}}$ and $\mu_{s_{\text{agar}}}$ for pure agar powder, we were able to calculate the $\mu_{a_{\text{coffee}}}$ and $\mu_{s_{\text{TiO2}}}$ for pure instant coffee and TiO_2 powders as well, which were calculated to be 19948 and 142950 m^{-1}, respectively. For this calculations we considered C_{coffee} and C_{TiO2} to be roughly 0.01 and 0.001 for 1.2% w/w instant coffee and 0.1% w/w TiO_2 agar gel samples, respectively. We assumed the refractive index of the samples to be equal to that for the water which is about 1.35 at 850 nm. The value for parameters as calculated in this part will be used in Sec. 6 to perform MC simulations.

4. EXPERIMENTS

The experimental set up can be seen in Fig. 3. In this set up, we used an 850 nm VCSEL (Litrax Technology Co., Ltd.) operating at 3.55 mA, just above the threshold current which is approximately 3.4 mA under feedback regime, temperature controlled at 35°C, and two lenses (C240TME-B, Thorlabs, Inc.) with both focal lengths and clear apertures of 8 mm to collimate and focus the laser beam. We used an optical chopper to modulate the

beam and extract the diffuse reflectance intensity modulated voltage signal from the VCSEL terminal voltage. The optical chopper modulated the laser beam at 877 Hz which prevented the steady state diffuse reflectance signal from being submerged in the low frequency noise of the semiconductor laser. Optical chopper created two operating states in the laser which are the free-running and under optical feedback states.[28] Diffuse reflectance signal can be obtained both from the time domain signal, by looking at two levels of signal corresponding to the two aforementioned states, or from the signal spectrum by looking at the magnitude of the first harmonic of the frequency domain signal. We extracted diffuse reflectance signal from the frequency domain and normalized the measured signals at all the points to the maximum value to make the images.

We raster scanned the skin tissue phantom which was prepared as discussed in Sec. 3, to make the images. We scanned an area of 6×6 mm with 41×41 steps with 150 μm step sizes. At each point we obtained the amplified laser diode terminal voltage signal using a data acquisition card. The three-layer skin tissue phantom can be seen in Fig. 2. As discussed earlier, a cover slip was placed on the top of the three-layer phantom to stop agar from evaporating. It also suppressed the effect of strong surface reflection between the air and sample. Surface reflection from the cover slip was specular which was less likely to be backscattered into the laser cavity as it needed perfect alignment which we deliberately avoided in the experiment which is also challenging to achieve in an LFI system.

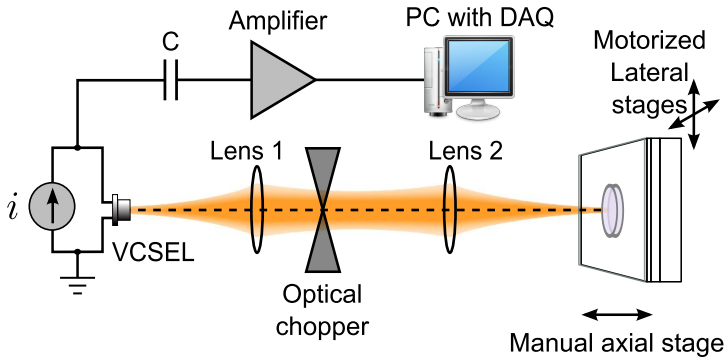

Figure 3. Experimental set up; laser feedback interferometry system raster scanning a three-layer skin tissue phantom including a KSC area.

5. EXPERIMENTAL RESULTS

Figure 4 shows the results of the experimental scans of the three-layer agar tumorous skin tissue which was prepared as discussed in Sec. 3 using the proposed LFI diffuse reflectance imaging technique. We scanned the tumorous model at eight different depths starting from above the tumorous area into the tumorous region to show the possibility of depth sectioning into the model. Scans started at the depth of about 280 μm from the surface of the first agar layer by adjusting the focal point at this depth and completing a lateral scan. We continued to perform the other scans by focusing into the agar sample at 100 μm length incremental steps which was equivalent to about 135 μm optical length incremental steps, as the refractive index of the agar gel was taken to be 1.35. In other words, considering the surface of the first agar gel as the reference, the scans took place at eight different depths of 280, 415, 550, 685, 840, 955, 1090, and 1225 μm which are shown in Figs. 4 (a), (b), (c), (d), (e), (f), (g), and (h), respectively. The sample was mounted on a 3-axis translation stage with two motorized lateral stages and one manual axial stage along the laser beam. Then after accomplishing each lateral scan which produced an image, we manually moved the sample toward the laser using the axial stage by 100 μm which was equal to 135 μm optical length. All images then were normalized to the maximum recorded level of diffuse reflectance at each step. As discussed earlier, the thickness of the first layer was 500 μm and the tumorous model region was a 4 mm diameter cylindrical area enclosed in the second layer with the thickness of 1000 μm. Therefore the two first scans took place above the tumorous area which resulted in noise-like images which are illustrated in Figs. 4 (a) and (b), respectively. The third scan was perform at the depth of 550 μm

and it can be seen in Fig. 4 (c) that the tumorous model region started to show itself at a lower level of diffuse reflectance compared to the surrounding area. As we continued to focus into the sample, the lower scattering tumorous model region manifested itself clearly in the provided images. Although all the other scans situated into the tumorous model area, as we focused deeper into the sample the signal started to fade out which was because of signal attenuation due to longer depth of scan.

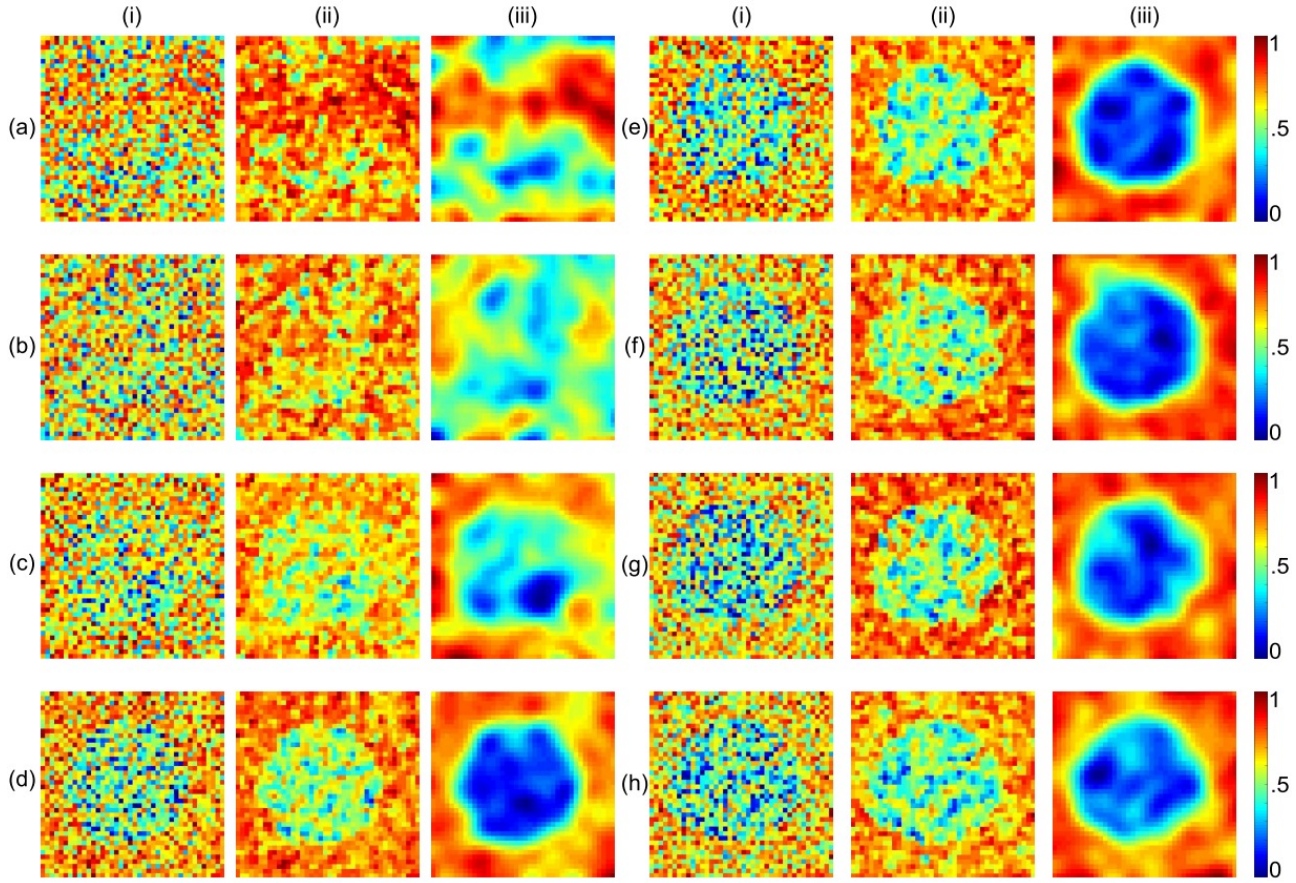

Figure 4. Laser feedback interferometry diffuse reflectance imaging experimental results; sub-figures of (a) to (h) illustrate the scan results at the focal depths of 280, 415, 550, 685, 840, 955, 1090, and 1225 μm from the surface of the first agar layer, respectively. (i)s show raw self-mixing image, (ii)s show the two dimensional median filtered image, and (iii)s show the two dimensional Gaussian filtered image.

The columns labeled as (i), (ii), and (iii) in Fig. 4 show raw, median filtered, and Gaussian filtered images, respectively. In other words, (i) is the image which was formed using the recorded self-mixing signal as it was obtained from the data acquisition card, (ii) was the raw image after applying a two dimensional median filter in Matlab, and (iii) was the raw image after applying a Gaussian filter in Matlab. Results show that our proposed technique can be used effectively in revealing the alterations in the optical properties of a tissue model non-invasively.

6. MONTE CARLO RESULTS

Monte Carlo is the name for a range of powerful simulation methods with a broad range of application which has also been used extensively in the field of modeling light–tissue interactions.[29–31] To interpret the experimental results obtained from laser feedback interferometry diffuse reflectance imaging technique, scanning a three-layer agar gel tumorous skin model, we numerically modeled the system by means of a MC simulation engine. Our

MC model consisted of the optical system model, photon population, and a three-layer tumorous skin model. We started the simulation by defining a Gaussian distribution of photons on the objective lens. About 2.5 million photons were included in the numerical model at each point which were characterized based on the specifications of the laser we used to conduct the experiments in Sec. 4.

We defined the geometrical and optical characteristics of the three-layer tumorous skin model in the simulation based on the properties of the agar gel sample that we described in Sec. 3. That is, the first layer in the numerical skin model was started with a 150 μm thick layer, modeling the cover slip, with scattering and absorption coefficients of zero. The second layer in the simulation was a 500 μm thick layer as the epidermis layer model, equivalent to an agar gel layer doped with about 1% volume proportion of instant coffee. The third layer in the simulation was a 1000 μm thick layer modeling the dermis layer, equivalent to an agar gel layer doped with about 0.1% volume proportion of TiO_2 enclosing a 4 mm diameter cylindrical lower scattering area in the middle. The fourth and final layer in the simulation was a 3.15 mm thick layer as the subcutaneous tissue model, equivalent to a pure agar layer. We defined basic scattering and absorption coefficients for all the three skin model layers equal to the values calculated in Sec. 3 for about 1% volume proportion of agar gel which were 65.85 and 0.5 m^{-1} for scattering and absorption coefficients, respectively. Then the extra optical properties due to the addition of TiO_2 and instant coffee were added to the basic optical properties. Scattering and absorption coefficients for TiO_2 were taken to be 142950 and 0 m^{-1}, respectively, and for instant coffee were taken to be 0 and 19948 m^{-1}, respectively, as measured in Sec. 3. We approximated the refractive index of all the layers including the cover slip to be 1.35 and the Henyey–Greenstein phase function with anisotropy factor of 0.85 was also considered to calculate the new direction of photons in the case of scattering events.[32,33]

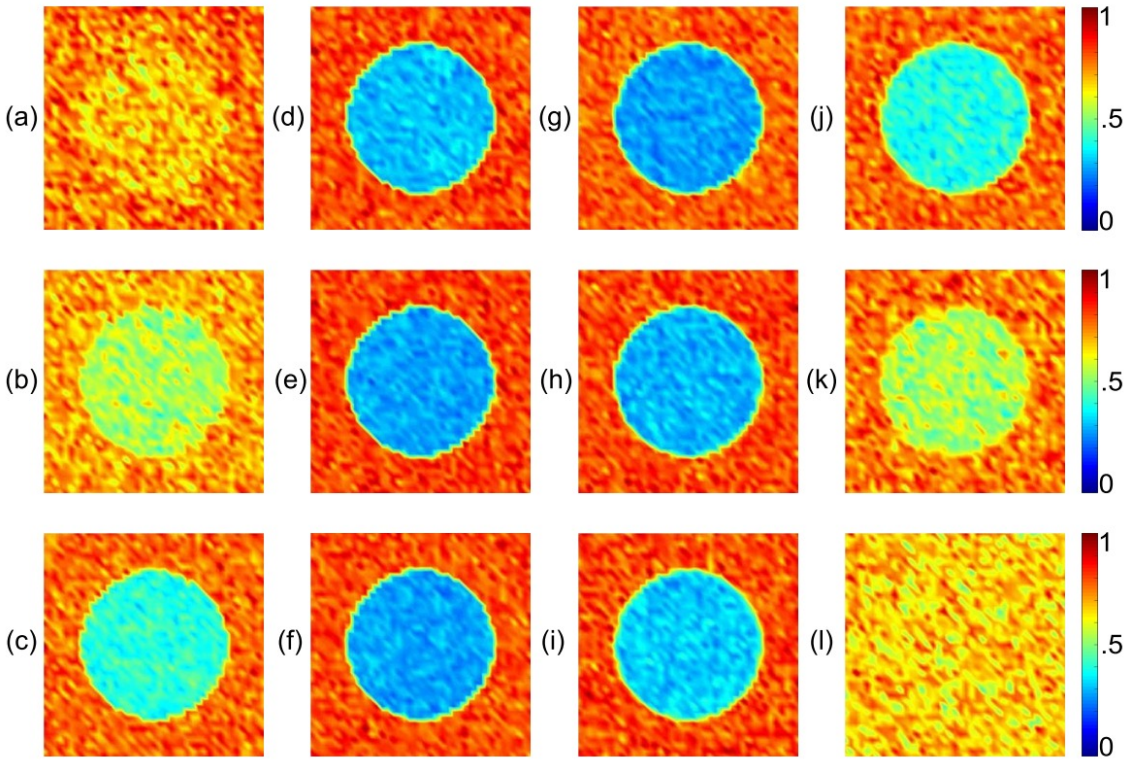

Figure 5. Monte Carlo simulation results for the three-layer tumorous skin model equivalent to the agar gel sample; sub-figures of (a) to (l) illustrate the simulated results at the focal plane depths of 185, 320, 455, 590, 725, 860, 995, 1130, 1265, 1400, 1535, and 1670 μm from the surface of the first skin layer model, respectively.

Photons enter the skin model and interact with the turbid media in the simulation. A small proportion of the photons travel back from the skin model and made their way back to the lens system. After performing ray

tracing method to model the path of photons interacting with the lens system, the ones which found their way to the laser aperture were counted as a measure of diffuse reflectance level. To perform the ray tracing we defined the geometrical specifications of the lens system as it was used in the experiments conducted in Sec. 4. As with the experiments, simulations were also performed point by point by raster scanning the photon beam over the skin model to prepare the images. Furthermore, the area of simulated scans were 6×6 mm including 41×41 steps with 150 μm step sizes, similar to that for the experimental results.

Figure 5 depicts the simulated MC results at 12 different depths into the tumorous skin model. We started the first scan at the depth of about 185 μm into the tumorous skin model from the surface of the first skin layer and the result can be seen in Fig. 5 (a). We continued to scan by further depth sectioning. We moved the optical system numerically with 100 μm incremental steps which was equivalent to 135 μm optical length as the refractive index was considered to be 1.35. It means that the focal plane of the 12 scans laid at the depths of 185, 320, 455, 590, 725, 860, 995, 1130, 1265, 1400, 1535, and 1670 μm from the surface of the first skin layer model and the results of these numerical scans are shown in Figs. 5 (a) to (l), respectively. In the MC simulation, tumorous skin model was situated between the depths of 500 to 1500 μm. Therefore, the first three scans which were (a) to (c) and the last two scans which were (k) and (l) took place outside the tumorous area and it is clearly seen from Fig. 5 that images at these depths have lower contrast compared to the scans inside the tumorous area which are (d) to (j). Although the scans in Figs. 5 (b), (c), and (k) were performed at the depths outside the tumorous region, we are still able to see noisy images of the circular tumorous area as the sensing volume in the simulations at these depths were extended into the tumorous region. The simulated results in this section shows consistency with the experimental results in Sec. 4 and enables us to investigate the new possibilities and implementations of the technique in further research.

7. CONCLUSION

Keratinocyte skin cancer, in particular basal cell carcinoma and squamous cell carcinoma are the most frequently observed malignancies in the fair-skinned population.[34,35] The most important factor in the development of KSC is exposure to increased ultra-violet radiation while skin phenotype also plays an important role.[34] These kind of neoplastic skin diseases often develop from pre-existed skin lesions. As an example actinic keratoses are the most common precursors to squamous cell carcinomas.[17] Diagnosis of KSC in early stages is challenging as human skin has a large surface and it is susceptible to numerous diseases. Some of them may resemble one type of skin cancer closely. Laser and other optical imaging techniques based on functional and structural modalities of skin tissue which are able to provide in-depth images of skin tissue are promising tools to be used in early skin cancer detection compared to conventional techniques such as using a dermascope and histopathological tests.

In this paper we proposed a new technique of diffuse reflectance imaging in the near-infrared region with applications in *in vivo* biological tissue imaging and skin cancer detection. We proposed a compact, low-cost, self-aligned, and versatile LFI system in a confocal configuration. The confocal set up allowed to perform depth sectioning in preparing the images. To examine the technique we applied it to a three-layer skin tissue phantom and performed MC simulation of the experimental set up including the numerical model of the skin phantom. The skin tissue phantom was made up of agar gel dope with absorbers and scatterers to control the optical properties and included a 4 mm diameter cylindrical lower scattering region encapsulated in the second layer which resembled a KSC. We provided eight images from the skin tissue phantom at different depths into the sample by 135 μm optical incremental steps. A high degree of consistency exists between experimental and computational results which validated the theoretical base of the technique to be used in such purposes and the capability of the technique to produce sensitive images of the lower scattering region at different depths and with a penetration depth of well over 1.2 mm into the skin phantom.

This research was supported under Australian Research Councils Discovery Projects funding scheme (DP 160 103910). The first author would also like to thank The University of Queensland Graduate School International Travel Award for financial support in preparing this work.

REFERENCES

[1] Weissleder, R., "A clearer vision for in vivo imaging," *Nature Biotechnology* **19**(4), 316–317 (2001).

[2] Garcia-Uribe, A., Zou, J., Duvic, M., Cho-Vega, J. H., Prieto, V. G., and Wang, L. V., "In vivo diagnosis of melanoma and nonmelanoma skin cancer using oblique incidence diffuse reflectance spectrometry," *Cancer Research* **72**(11), 2738–2745 (2012).

[3] Bashkatov, A., Genina, E., Kochubey, V., and Tuchin, V., "Optical properties of human skin, subcutaneous and mucous tissues in the wavelength range from 400 to 2000 nm," *Journal of Physics D: Applied Physics* **38**(15), 2543 (2005).

[4] Salomatina, E., Jiang, B., Novak, J., and Yaroslavsky, A. N., "Optical properties of normal and cancerous human skin in the visible and near-infrared spectral range," *Journal of Biomedical Optics* **11**(6), 064026–064026 (2006).

[5] Farrell, T. J., Patterson, M. S., and Wilson, B., "A diffusion theory model of spatially resolved, steady-state diffuse reflectance for the noninvasive determination of tissue optical properties invivo," *Medical Physics* **19**(4), 879–888 (1992).

[6] Mourant, J. R., Hielscher, A. H., Eick, A. A., Johnson, T. M., and Freyer, J. P., "Evidence of intrinsic differences in the light scattering properties of tumorigenic and nontumorigenic cells," *Cancer Cytopathology* **84**(6), 366–374 (1998).

[7] Dögnitz, N. and Wagnières, G., "Determination of tissue optical properties by steady-state spatial frequency-domain reflectometry," *Lasers in Medical Science* **13**(1), 55–65 (1998).

[8] Doornbos, R., Lang, R., Aalders, M., Cross, F., and Sterenborg, H., "The determination of in vivo human tissue optical properties and absolute chromophore concentrations using spatially resolved steady-state diffuse reflectance spectroscopy," *Physics in Medicine and Biology* **44**(4), 967 (1999).

[9] Woodward, R. M., Cole, B. E., Wallace, V. P., Pye, R. J., Arnone, D. D., Linfield, E. H., and Pepper, M., "Terahertz pulse imaging in reflection geometry of human skin cancer and skin tissue," *Physics in Medicine and Biology* **47**(21), 3853 (2002).

[10] Guo, B., Wang, Y., Peng, C., Zhang, H., Luo, G., Le, H., Gmachl, C., Sivco, D., Peabody, M., and Cho, A. Y., "Laser-based mid-infrared reflectance imaging of biological tissues," *Optics Express* **12**(1), 208–219 (2004).

[11] Hofmann-Wellenhof, R., Pellacani, G., Malvehy, J., and Soyer, H. P., [*Reflectance confocal microscopy for skin diseases*], Springer Science & Business Media (2012).

[12] Giuliani, G., Norgia, M., Donati, S., and Bosch, T., "Laser diode self-mixing technique for sensing applications," *Journal of Optics A: Pure and Applied Optics* **4**(6), S283 (2002).

[13] Donati, S. and Norgia, M., "Self-mixing interferometry for biomedical signals sensing," *Selected Topics in Quantum Electronics, IEEE Journal of* **20**(2), 104–111 (2014).

[14] Taimre, T., Nikolić, M., Bertling, K., Lim, Y. L., Bosch, T., and Rakić, A. D., "Laser feedback interferometry: a tutorial on the self-mixing effect for coherent sensing," *Advances in Optics and Photonics* **7**(3), 570–631 (2015).

[15] Lu, C.-H., Wang, J., and Deng, K.-L., "Imaging and profiling surface microstructures with noninterferometric confocal laser feedback," *Applied Physics Letters* **66**(16), 2022–2024 (1995).

[16] Juškaitis, R., Rea, N., and Wilson, T., "Semiconductor laser confocal microscopy," *Applied Optics* **33**(4), 578–584 (1994).

[17] Sober, A. J. and Burstein, J. M., "Precursors to skin cancer," *Cancer* **75**(S2), 645–650 (1995).

[18] Schwartz, R., Bridges, T., Butani, A., and Ehrlich, A., "Actinic keratosis: an occupational and environmental disorder," *Journal of the European Academy of Dermatology and Venereology* **22**(5), 606–615 (2008).

[19] Anderson, R. R. and Parrish, J. A., "The optics of human skin," *Journal of Investigative Dermatology* **77**(1), 13–19 (1981).

[20] Kliese, R., Taimre, T., Bakar, A. A. A., Lim, Y. L., Bertling, K., Nikolić, M., Perchoux, J., Bosch, T., and Rakić, A. D., "Solving self-mixing equations for arbitrary feedback levels: a concise algorithm," *Applied Optics* **53**(17), 3723–3736 (2014).

[21] Acket, G. A., Lenstra, D., Den Boef, A. J., and Verbeek, B. H., "The influence of feedback intensity on longitudinal mode properties and optical noise in index-guided semiconductor lasers," *Quantum Electronics, IEEE Journal of* **20**(10), 1163–1169 (1984).

[22] Spencer, P., Rees, P., and Pierce, I., "Theoretical analysis," in [*Unlocking Dynamical Diversity: Optical Feedback Effects on Semiconductor Lasers*], Kane, D. M. and Shore, K. A., eds., ch. 2, John Wiley & Sons (2005).

[23] Lim, Y. L., Bertling, K., Rio, P., Tucker, J., and Rakic, A., "Displacement and distance measurement using the change in junction voltage across a laser diode due to the self-mixing effect," in [*Microelectronics, MEMS, and Nanotechnology*], 60381O–60381O, International Society for Optics and Photonics (2005).

[24] Anderson, R. and Parrish, J., "Optical properties of human skin," in [*The Science of Photomedicine*], 147–194, Springer (1982).

[25] Cubeddu, R., Pifferi, A., Taroni, P., Torricelli, A., and Valentini, G., "A solid tissue phantom for photon migration studies," *Physics in Medicine and Biology* **42**(10), 1971 (1997).

[26] Pogue, B. W. and Patterson, M. S., "Review of tissue simulating phantoms for optical spectroscopy, imaging and dosimetry," *Journal of biomedical optics* **11**(4), 041102–041102 (2006).

[27] Nishidate, I., Aizu, Y., and Mishina, H., "Estimation of melanin and hemoglobin in skin tissue using multiple regression analysis aided by monte carlo simulation," *Journal of Biomedical Optics* **9**(4), 700–710 (2004).

[28] Bertling, K., Taimre, T., Agnew, G., Lim, Y. L., Dean, P., Indjin, D., Hoefling, S., Weih, R., Kamp, M., von Edlinger, M., et al., "Simple electrical modulation scheme for laser feedback imaging," *IEEE Sensors Journal* **16**, 1937–1942 (2016).

[29] Tuchin, V., [*Tissue optics: light scattering methods and instruments for medical diagnosis*], SPIE press, Bellingham, Washington USA (2007).

[30] Wang, L., Jacques, S. L., and Zheng, L., "MCML–Monte Carlo modeling of light transport in multi-layered tissues," *Computer Methods and Programs in Biomedicine* **47**(2), 131–146 (1995).

[31] Mowla, A., Nikolić, M., Taimre, T., Tucker, J. R., Lim, Y. L., Bertling, K., and Rakić, A. D., "Effect of the optical system on the doppler spectrum in laser-feedback interferometry," *Applied Optics* **54**(1), 18–26 (2015).

[32] Hammer, M., Yaroslavsky, A. N., and Schweitzer, D., "A scattering phase function for blood with physiological haematocrit," *Physics in Medicine and Biology* **46**(3), N65 (2001).

[33] Fredriksson, I., Larsson, M., and Strömberg, T., "Optical microcirculatory skin model: assessed by Monte Carlo simulations paired with in vivo laser Doppler flowmetry," *Journal of Biomedical Optics* **13**(1), 014015–014015 (2008).

[34] Soyer, H. P., Rigel, D., and Wurm, E. M., [*Dermatology*], ch. Actinic Keratosis, Basal Cell Carcinoma and Squamous Cell Carcinoma, 1773–1794, London: Elsevier, 3rd ed. (2012).

[35] Baldi, A., Pasquali, P., and Spugnini, E. P., [*Skin Cancer: A Practical Approach*], Humana Press, Springer (2014).